ELSEVIER

Combustion and Flame 135 (2003) 503–523

Combustion and Flame

Generation of PDFS for flame curvature and for flame stretch rate in premixed turbulent combustion

D. Bradley[a,*], P. H. Gaskell[a], A. Sedaghat[a], X. J. Gu[b]

[a]*School of Mechanical Engineering, University of Leeds, Leeds LS2 9JT, England*
[b]*Department of Computational Science and Engineering, CLRC Daresbury Laboratory, Warrington WA4 4AD, England*

Received 15 February 2003; received in revised form 26 June 2003; accepted 16 July 2003

Abstract

Experimentally derived pdfs of turbulent, premixed, flame curvatures from a variety of sources, for a wide range of conditions are surveyed and a suitable expression sought to generalize these. This proves to be one based on the Damköhler number, *Da*. This is tantamount to normalizing the curvature by multiplying it by the Taylor scale of turbulence. It enables the distribution of flame curvature when normalized by the laminar flame thickness, to be expressed in terms of the Karlovitz stretch factor, *K*, and the turbulent Reynolds number, R_l. The value of the pdf at zero curvature is linearly related to $Da^{1/2}$.

The pdf expressions of Yeung et al. [3] obtained from numerical simulations are used for the strain rate distribution and, on the assumption that these and that for flame curvature are statistically independent, values of flame stretch rate pdfs are generated numerically. It is necessary to define an appropriate surface to define the burning velocity, flame stretch rate, and appropriate Markstein numbers. Two surfaces are considered and employed in the computations, one located at the start of the preheat zone, the other at the start of the reaction zone. The latter seems more rational and gives the better generalisation of the pdfs of flame stretch rate.

An assumed linearity of laminar burning velocity with flame stretch rate, extending over both positive and negative stretch rates, enables flame stretch rate pdfs to be generated. It is concluded that negative values of burning velocity are unlikely and that burning velocities should tend to zero rather than attain negative values. This modifies the derivation of flame stretch rate pdfs. These depend on the Markstein number, Karlovitz stretch factor and turbulent Reynolds number. Computations suggest that, for values of *K* above 0.1 and of R_l above 100, the pdf of stretch rate is similar to that of strain rate. At very low values of *K* and negative values of Markstein number, pronounced flamelet instability might be anticipated.

Keywords: Turbulent combustion; Probability density function; Stretch rate

1. Introduction

The stretch rate, to which a flame is subjected is important in determining the burning rate and whether the flame might be extinguished. For a flame of surface area, *A*, its stretch rate is given by [1]:

$$\frac{1}{A}\frac{dA}{dt} = -\mathbf{n}\,\mathbf{n}\colon \nabla\mathbf{u} + \nabla\cdot\mathbf{u} + u_n\nabla\cdot\mathbf{n}. \qquad (1)$$

Here *u* and u_n are, respectively, the local gas velocity and the stretched laminar burning velocity normal to the flame surface, with *n* a unit vector normal to the surface directed from the burned to the unburned

* Corresponding author. Tel.: +44-113-243-1751; fax: +44-113-242-4611.
E-mail address: d.bradley@leeds.ac.uk (D. Bradley).

0010-2180/03/$ – see front matter
doi:10.1016/S0010-2180(03)00181-0

Nomenclature

A	Flame surface area
a	Power function constant, see Table 2
a_c	Normalized flame curvature component of flame stretch rate
a_s	Normalized strain rate component of flame stretch rate
$\bar{a}_s$	Normalized mean strain rate
b	Power function constant, see Table 2
C	Numerical constant in Eqs. 19 and 22
C_h	Physico-chemical parameter expression in Eq. 2
Da	Damköhler number
$f(x_i)$	Fitting curve function
h	Flame curvature
K	Turbulent Karlovitz stretch factor
Ka	Karlovitz number ($= \sqrt{15}\ K$)
l	Integral length scale of turbulence
L_c	Markstein length for stretch rate because of curvature
L_s	Markstein length for strain rate
Le	Lewis number
Ma_c	Markstein number for stretch rate because of curvature
Ma_{cp}	Markstein number for stretch rate because of curvature, based on preheat zone surface
Ma_{cr}	Markstein number for stretch rate because of curvature, based on reaction zone surface
Ma_s	Markstein number for strain rate
Ma_{sp}	Markstein number for strain rate, based on preheat zone surface
Ma_{sr}	Markstein number for strain rate, based on reaction zone surface
M_d	Markstein number used in [7]
$\mathbf{n}$	Unit vector
n	Number of data points
Pe	Peclet number
Pe_{cl}	Critical Peclet number
$p_2(a_s)$	Pdf of normalized strain rate
$p_1(h\delta_\ell)$	Pdf of normalized flame curvature
$p(hx)$	Normalised pdf of flame curvature
$p_3(s)$	Pdf of normalized flame stretch rate
$p(s, x)$	Joint pdf of normalized flame stretch rate and x
R_l	Turbulent Reynolds number based on integral length scale of turbulence
R_λ	Turbulent Reynolds number based on Taylor length scale of turbulence
r	Correlation coefficient. Also spherical flame radius
S_r	Standard deviation for fitting curve
S_t	Standard deviation
s	Normalised flame stretch rate
s_c	Normalised flame stretch rate at which $u_n/u_\ell = 0$
t	Time
u'	Rms turbulent velocity
u	Local gas velocity
u_ℓ	Unstretched laminar burning velocity
u_n	Stretched laminar burning velocity
v_η	Kolmogorov velocity
x	Normalising length for flame curvature. Also dummy variable in Eq. 28
y_i	Data point value
$\bar{y}$	Mean of data points
δ_ℓ	Laminar flame thickness given by ν/u_ℓ
ε	Mean rate of dissipation of turbulent energy
η	Kolmogorov turbulence length scale
λ	Taylor length scale of turbulence
ρ_u/ρ_b	Ratio of unburned/burned gas density
τ	$\rho_u/\rho_b - 1$
ν	Kinematic viscosity
σ_s	Normalised rms strain rate
τ_η	Kolmogorov time scale

side. The first two terms on the right comprise the strain rate tensor (tangential strain rate) and the third the flame stretch rate because of flame curvature (stretched laminar burning velocity × flame curvature). The equation is that of a surface and because of the finite flame thickness, complications, discussed later, arise in the selection of the most appropriate one [2].

For turbulent flames there is a distribution of stretch rates. To some degree, the effects of positive

and negative curvatures cancel and the rate of strain component tends to dominate. If the flame curvature term in Eq. 1 is neglected the flame stretch rate is given by the strain rate tensor. The probability density function (pdf) of the strain rate has been obtained by Yeung et al. [3] from direct numerical simulations (DNS) in non-reacting mixtures, for both material and random surfaces. In both cases the pdf is of an asymmetric, near-Gaussian form. Although the strain rate contribution usually is the dominant one in turbulent flow, it is important to know how the flame stretch rate pdf might differ from that of the strain rate.

Some pdfs of flame stretch rate have been obtained from DNS of flames but, because of computational limitations, usually these have been limited to low Reynolds numbers and simple chemical kinetics. In a two-dimensional DNS study of the effects of stretch rate in turbulent CH_4-air mixtures, with a detailed C_1 mechanism, Chen and Im [4] obtained pdfs of both strain rate and flame stretch rate. The shape of the former was close to that obtained by Yeung et al. [3]. The principal difference between the two pdfs was a long tail of negative stretch rate, attributable to the flame curvature term in Eq. 1. This regime with a highly negative stretch rate (compression) combined with high positive curvature was also observed experimentally by Renou et al. [5]. The influence of a negative stretch rate on flames is difficult to assess, because flames stretched in this way are inherently unstable and consequently difficult to study.

Earlier numerical simulations by Rutland and Trouvé [6] at constant density with single step Arrhenius kinetics yielded strain rate pdfs at different Lewis numbers, *Le*. Independently of the value of *Le*, the simulations yielded about a 20% probability of a negative strain rate and a mean strain rate that were in good agreement with the values of Yeung et al. [3]. Also presented were pdfs of flame curvature and these were slightly negatively skewed.

In an important development Kostiuk and Bray [7] combined the pdfs of strain and curvature, previously obtained from constant density numerical simulations with single step Arrhenius kinetics [8], to obtain pdfs of flame stretch rate. Results were presented for different Markstein numbers and Karlovitz stretch factors and they suggested a 30–50% probability of negative flame stretch rate.

There are few data on the direct contribution of the flame curvature term to the flame stretch rate, although data are available on the more readily accessible distributions of flame curvature. Consequently, the first stage in the present derivation of the desired pdf of stretch rates was to elucidate the contribution of curvature to this, perforce via the available data on curvature distributions. Experimental data on flame curvature pdfs from a variety of sources first are scrutinised, followed by the derivation of an empirical expression for a universal pdf of curvature. The curvature contribution to the flame stretch rate is obtained from the curvature and an expression for the burning velocity ratio, u_n/u_ℓ. Following Kostiuk and Bray, this is combined with an expression for the strain rate pdf and numerical solutions are obtained for pdfs of flame stretch rate for different Karlovitz, Reynolds, and Markstein numbers. It will be shown that for many practical combustion regimes; the flame stretch rate pdf is close to the strain rate pdf. Such pdfs enable values of the probablity of burning function, P_b, [9] and the flame stretch factor, I_o, [7] to be evaluated in flamelet modeling of turbulent combustion.

2. Flame curvature PDFS

The experimental data employed comprise the planar laser-induced fluoresence (PLIF) measurements of Haq et al. [10] for turbulent premixed isooctane-air and methane-air explosion flames in a fan stirred bomb at pressures of 0.1 and 0.5 MPa, the Rayleigh laser sheet measurements of Shepherd et al. [11], for lean premixed methane-air flames on a low swirl burner with quasi-isotropic turbulence, the particle image velocimetry (PIV) and PLIF diagnostics of Nye et al. [12] in lean methane/air V-flames interacting with a vortex sheet, and the PLIF measurements of Lee et al. [13] on turbulent pulsed flames. Curvatures could be measured along contours representing different values of the reaction progress variable, but Shepherd et al. [11] have shown the derived pdf of curvatures shows little dependence on these values.

The experimental conditions surveyed, which extend over an appreciable range of Damköhler number, *Da*, and Markstein number based on the rate of strain and the rate of formation of burned gas, Ma_{sr}, [2], are summarized in Table 1. Altogether a total of 25 pdfs were considered. The experimentally measured values of eight of these, spread throughout the range, are shown in order of decreasing *Da* (increasing turbulence), by the symbols in Fig. 1. In this instance the curvature is normalized by multiplying it by the flame thickness, δ_ℓ, given by ν/u_ℓ. Other normalizing lengths are considered later. In [7] Kostiuk and Bray normalized with the Kolmogorov length scale, η.

The maximum measurable value of curvature, *h*, was determined by pixel size and this was 1.7 mm^{-1} in [10] and 2 mm^{-1} in [12]. Reference to Table 1 shows the smallest value of δ_ℓ was 0.012 mm in

Table 1
Turbulent flame characteristics associated with measured pdfs of flame curvature

Fuel	ϕ	Da	K	Ma_{sr}	R_l	u'/u_ℓ	ν (m^2/s) $\times 10^6$	δ_ℓ (mm)	η (mm)	λ (mm)
i-$C_8H_{18}^+$	1.00	465	0.041	4.00	5680	3.49	39.4	0.012	0.03	1.06
i-C_8H_{18}	1.00	368	0.016	6.00	568	1.24	197	0.044	0.17	3.36
i-C_8H_{18}	0.75	257	0.023	13.0	555	1.47	201	0.053	0.18	3.39
i-$C_8H_{18}^+$	0.75	235	0.079	3.00	5550	4.86	40.3	0.018	0.03	1.07
i-C_8H_{18}	1.00	184	0.046	6.00	1140	2.48	197	0.044	0.10	2.37
i-C_8H_{18}	1.40	180	0.033	−1.00	548	1.75	204	0.064	0.18	3.42
CH_4	1.00	160	0.053	4.20	1160	2.69	193	0.046	0.10	2.35
i-$C_8H_{18}^+$	1.00	155	0.210	4.00	17000	10.5	39.4	0.012	0.01	0.61
i-C_8H_{18}	0.75	128	0.065	13.0	1110	2.94	201	0.053	0.11	2.40
CH_4[12]	0.70	119	0.052	2.68	600	2.25	150	0.075	0.17	3.27
CH_4	0.70	115	0.053	2.70	598	2.28	187	0.076	0.17	3.27
C_3H_8[13]	1.00	97	0.036	5.91	195	1.42	148	0.035	0.09	1.38
i-C_8H_{18}	1.40	90	0.092	−1.00	1100	3.49	204	0.064	0.11	2.42
C_3H_8[13]	1.25	82	0.039	2.45	164	1.42	146	0.042	0.11	1.50
C_3H_8[13]	0.75	79	0.040	6.10	159	1.42	151	0.043	0.11	1.52
i-C_8H_{18}	1.00	61	0.238	6.00	3410	7.45	197	0.044	0.05	1.37
CH_4	0.70	57	0.150	2.70	1196	4.56	187	0.076	0.10	2.31
CH_4[11]	0.70	54	0.120	2.68	656	3.50	160	0.080	0.55	6.53
CH_4	1.00	53	0.277	4.20	3480	8.08	193	0.046	0.04	1.36
i-C_8H_{18}	1.40	45	0.261	−1.00	2190	6.99	204	0.064	0.06	1.71
i-C_8H_{18}	0.75	43	0.337	13.0	3330	8.83	201	0.053	0.05	1.39
i-C_8H_{18}	1.00	37	0.512	6.00	5680	12.4	197	0.044	0.03	1.06
i-C_8H_{18}	1.40	30	0.479	−1.00	3290	10.5	204	0.064	0.05	1.40
CH_4	0.70	19	0.782	2.70	3590	13.7	187	0.076	0.04	1.34
CH_4[11]	0.70	10	1.476	2.68	3510	18.7	160	0.080	0.03	1.01

i-C_8H_{18}: iso-octane-air, CH_4: methane-air, C_3H_8: propane-air.

All mixtures are with air and at 0.1 MPa, except where "+" indicates 0.5 MPa. Unless otherwise indicated, data are from [10]. Superscript in first column indicates other reference. For [10] l = 20 mm, for [11] l = 15 mm, and l = 4.8 mm for [12] and [13]. Flame thickness found from $\delta_\ell = \nu/u_\ell$.

measurements at 0.5 MPa, so that at this pressure values of $h\ \delta_\ell$ in Fig. 1 ($Da = 465$) could only be reliable up to about 0.021 which, in this instance, is probably restrictive. On the other hand, most of the measurements were at 0.1 MPa and, at the larger values of δ_ℓ, they are much less restrictive. For example, at the highest values of δ_ℓ at this pressure, namely 0.08 mm, and again with a maximum value of h of 1.7 mm^{-1}, the maximum value of $h\ \delta_\ell$ is 0.136 for the data in [10]. Reference to Fig. 1 suggests there are only very small contributions to the pdf at values greater than this. That there may be some contribution is shown by Fig. 1 ($Da = 10$ and $Da = 54$). These data from [11] are derived from better spatial resolutions, with 23 compared with 6 pixels/mm in [10]. The figures suggest a consequent limiting value of $h\delta_\ell$ of about 0.5 and that these particular pdfs are fully resolved.

Negative values of Ma_{sr} would encourage cusp formation, with highly negative curvature [14]. Scrutiny of the measured pdfs suggested there was no obvious influence of Ma_{sr}, although Haq et al. [10] found that the flames most influenced by stretch rate, with high positive values of Ma_{sr}, had smoothed-out cusps. Less stable flames, with low or negative values of Ma_{sr} displayed sharp cusps with, in extreme cases, quenching at the tip. This is a consequence of the combined influence of negative stretch rates and negative Markstein numbers. Lee et al. [13] found the wrinkled flame perimeter to be greater for the less stable flames.

Fig. 1 also suggests that the measured mean curvatures are very close to zero, with a very slight skew to negative curvatures, at the higher values of D_a, [8,11]. There is no discernible general trend in skewness with Da and curve-fitting to a symmetric Gaussian expression seemed to be justified. Consequently, following Haq et al. [10], the pdf of normalized curvature, $p(hx)$, is assumed to be of symmetric Gaussian form

$$p(hx) = \frac{1}{C_h\sqrt{2\pi}} \exp\left[-\frac{1}{2}\left(\frac{hx}{C_h}\right)^2 \right], \qquad (2)$$

notwithstanding that this might mask the presence of some negative curvature at cusps. Here x is an ap-

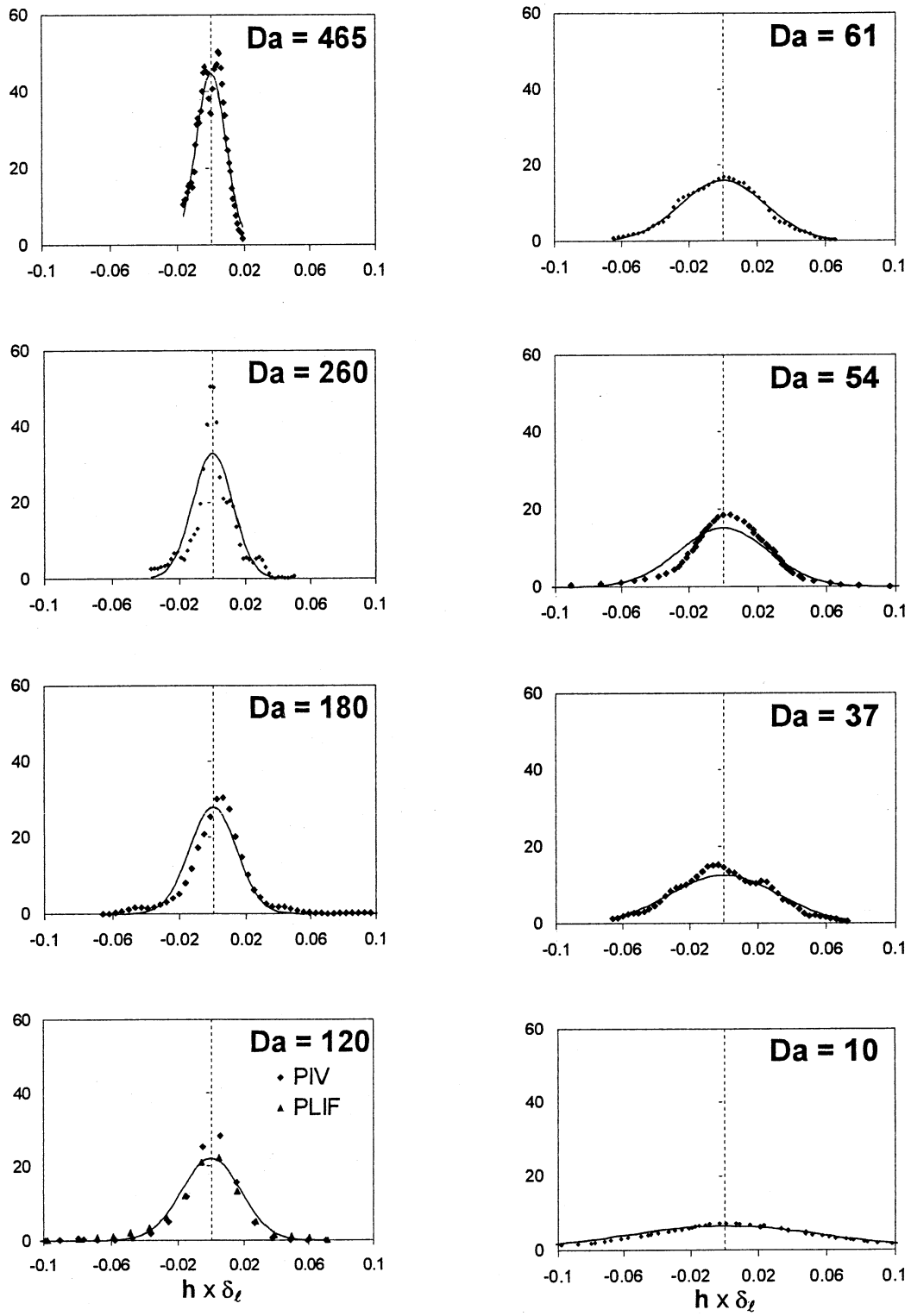

Fig. 1. Pdfs of normalized flame curvature at different Damköhler numbers. Symbols: normalized experimental curvatures, ($h\delta_\ell$). Full line curve: Eq. 10.

Table 2
Summary of correlating power functions for Gaussian coefficient, C_h, using different normalized pdfs of curvature

Normalizing scale, x	$C_h = a \cdot K^b$			$C_h = a \cdot Da^b$			$C_h = a \cdot Da^{0.5}$	
	a	b	r	a	b	r	a	r
δ_ℓ	0.045	0.310	0.857	0.168	−0.463	0.946	0.192	0.942
λ	0.751	−0.018	0.137	0.803	−0.006	0.034	5.011	2.619
η	0.024	−0.184	0.582	0.021	0.124	0.290	0.220	1.368

propriate normalising length scale for the curvature, h, and C_h is a function of an appropriate physico-chemical parameter.

The unstretched laminar flame thickness, δ_ℓ, the Taylor length scale of turbulence, λ, and the Kolmogorov length scale, η, were all considered as possible normalising parameters, x, in attempts to find the best generalised pdf. These lengths were given by $\delta_\ell = \nu/u_\ell$, $\lambda/l = 4/\sqrt{R_l}$, in which R_l is the turbulent Reynolds number based on the integral length scale, l, and $\eta/l = 2/(15R_l^3)^{1/4}$. With regard to the C_h function, it might be expected that the curvature is influenced by the Karlovitz stretch factor, the Damköhler, and turbulent Reynolds numbers.

The turbulent Karlovitz stretch factor, K, arises from the isotropic turbulence relationship

$$\left(\frac{\varepsilon}{15\nu}\right)^{1/2} = \frac{u'}{\lambda}, \tag{3}$$

in which ε is the mean rate of dissipation of turbulent energy and u'/λ is the rms strain rate on a randomly orientated surfaces [3]. When this rms strain rate is normalized by the chemical time, δ_ℓ/u_ℓ, it gives $K = (u'/\lambda)(\delta_\ell/u_\ell)$. With the above expressions for δ_ℓ and λ/l, this becomes

$$K = 0.25\,(u'/u_\ell)^2\, R_\ell^{-0.5}. \tag{4}$$

The Damköhler number, $Da = (l/u')(u_\ell/\delta_\ell)$. Clearly, $K = 0.25(u'/u_\ell)Da^{-0.5}$ and $KDa = 0.25R_l^{0.5}$.

Both K and Da were considered in attempts to obtain an optimal expression for C_h Sometimes, as in [7], a slightly different definition of Karlovitz number, Ka, is employed, with $Ka = (\delta_\ell/u_\ell)/\tau_\eta$. Here τ_η is the Kolmogorov time, given by [9]

$$\tau_\eta = \left(\frac{\lambda}{u'\sqrt{15}}\right). \tag{5}$$

It follows that $Ka = \sqrt{15}K$.

An iterative procedure was employed in these attempts to obtain an expression for the pdf of curvature over the full range of the experimental data. Because of the limited resolution of the curvature at 0.5 MPa, data at this higher pressure were omitted from the optimisation. Having decided upon the form of the Gaussian expression, the Levenberg-Marquardt (LM) [15] non-linear regression technique was employed to tune the function C_h to give the best fit to the experimental curvature pdfs. The technique combines the steepest-descent and a Taylor series method to obtain fast and reliable solutions iteratively for non-linear regressions. The algorithm allows for a smooth transition between the two methods as the iteration proceeds.

The "goodness" of the final fit is measured by a correlation coefficient, r. The standard deviation quantifies the spread of data about the mean and is

$$S_t = \sum_{i=1}^{n} (\bar{y} - y_i)^2, \tag{6}$$

where $\bar{y}$ is the mean of the data points, given by

$$\bar{y} = \frac{1}{n}\sum_{i=1}^{n} y_i. \tag{7}$$

The fitting function is $f(x_i)$ and the deviation from it is given by

$$S_r = \sum_{i=1}^{n} (y_i - f(x_i))^2. \tag{8}$$

This measures the spread of data about the fitting function. The "goodness of fit" is quantified by the normalized difference between S_t and S_r. The correlation coefficient is given by

$$r = \sqrt{\frac{S_t - S_r}{S_t}}. \tag{9}$$

For a perfect fit, the standard error of the estimate approaches $S_r = 0$ and r approaches unity. With $r = 0$, the spread of data about the fitting function is no better than the spread about the mean. A correlation coefficient greater than unity is indicative of a very poor fit.

The procedure adopted can be summarised by reference to Table 2. First, the normalizing parameter, x, was selected, followed by the C_h parameter, K or Da. A variety of curve-fitting functions of K and

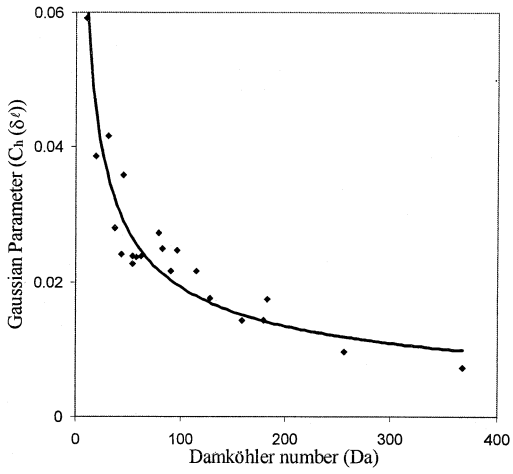

Fig. 2. Symbols: optimum value of C_h for each separate experimental pdf. Curve: correlation $C_h = 0.192\ Da^{-0.5}$ against *Da*.

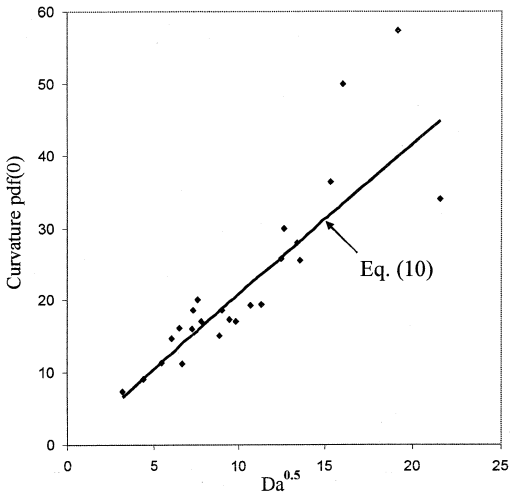

Fig. 3. Symbols: smoothed experimental values of curvature pdf at zero cuvature. Straight line: Eq. 10 at zero curvature.

Da, including linear, power, exponential, and logarithmic, were explored in turn, over the range of experimental data. It was found that the optimal correlation with the experimental pdfs occurred with a power function. Table 2 lists the optimum values for the constants *a* and *b* with three power functions for the three normalizing length scales, *x*. Also given in Table 2 are associated values of the correlation coefficient, *r*.

The best correlations were obtained with δ_ℓ as the normalizing length scale and with *Da* as a more appropriate physico-chemical parameter than *K*. The optimized expression was numerically rounded to give a power law of 0.5 for *Da*, such that the final optimized pdf of curvature became

$$p_1(h\delta_\ell) = \frac{1}{0.192Da^{-0.5}\sqrt{2\pi}} \exp\left[-\frac{1}{2}\left(\frac{h\delta_\ell}{0.192Da^{-0.5}}\right)^2\right], \quad (10)$$

for $470 \geq Da \geq 10$. This expression is plotted by the full line curves on Fig. 1.

The correlation $C_h = 0.192Da^{-0.5}$ is shown plotted against *Da* by the bold curve in Fig. 2. The symbols show the optimum value of C_h for each separate experimental pdf. Equation 10 suggests that at zero curvature the value of $p(\delta_\ell h)$ is proportional to $Da^{0.5}$. The symbols in Fig. 3 show smoothed experimental values at this value of the pdf and the full line curve values, given by Eq. 10, both plotted against $Da^{0.5}$. This is of interest in that, because the distribution of curvatures might be expected to govern the appearance of a flame, the appearance must be predominantly influenced by the Damköhler number.

Although Table 2 shows unsatisfactory correlation coefficients, *r*, with *x*, as λ, because $Da^{-0.5} = \delta_\ell/0.25\lambda$, an interesting alternative form for Eq. 10 is

$$p_1(h\lambda) = \frac{1}{0.77\sqrt{2\pi}} \exp\left[-\frac{1}{2}\left(\frac{h\lambda}{0.77}\right)^2\right]. \quad (11)$$

Here the curvature is normalized by the Taylor scale, as suggested by Lee et al. [13].

Another convenient and practical form of Eq. 10 is

$$p_1(h\delta_\ell) = \frac{2.6R_l^{0.25}}{K^{0.5}\sqrt{2\pi}} \exp\left(-\frac{1}{2}\left(\frac{2.6(h\delta_\ell)R_l^{0.25}}{K^{0.5}}\right)^2\right), \quad (12)$$

for $1.5 \geq K \geq 0.01$ and for $6000 \geq R_l \geq 150$.

This implies that the pdfs of flame stretch rate ultimately to be derived, will be functionally dependent upon *K* and R_l. Equation 12 will be used in the numerical derivation of the pdfs of the flame stretch rate. The influences of *K* and R_l on the curvature distribution given by this expression are shown in Fig. 4 for four values of *K* and a range of R_l values. The Reynolds number has a large influence on the pdf, whatever the value of *K*, but the influence of *K* declines for values above about 1.0. These pdfs were close to those in [7] only at the very low value of R_l equal to 0.66.

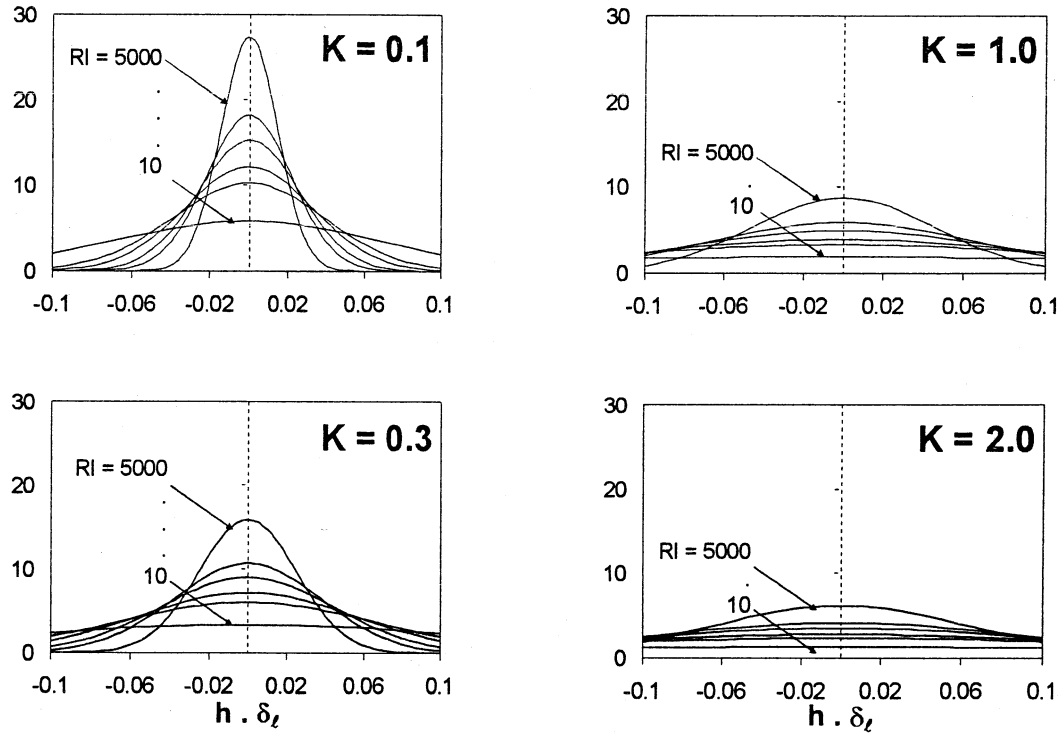

Fig. 4. Pdfs of normalized flame curvature given by Eq. 12, for different values of K and values of R_l of 5000, 1000, 500, 200, 100, and 10, in descending order.

3. Flame curvature contribution to the flame stretch rate

3.1. Dimensionless flame stretch rate

In [3] the strain rate in homogeneous turbulence is normalized by multiplying it by the Kolmogorov time, τ_η, given by Eq. 5, to give a dimensionless strain rate, a_s. The same procedure is followed in the present study and is extended to the curvature contribution and the overall stretch rate. The flame curvature contribution to the flame stretch rate, the last term in Eq. 1, is $2u_n h$, where u_n is the local, stretched, laminar, burning velocity [2]. When normalized by τ_η and denoted by a_c, it becomes

$$a_c = \left(\frac{\lambda}{u'\sqrt{15}}\right)2u_n h = \left(\frac{\lambda}{u'\sqrt{15}}\right)\left(\frac{u_\ell}{\delta_\ell}\right)\frac{2u_n}{u_\ell}h\delta_\ell = \frac{2u_n}{u_\ell}\frac{(h\delta_\ell)}{K\sqrt{15}}. \quad (13)$$

If s is the flame stretch rate normalized by the Kolmogorov time, then

$$s = a_s + a_c. \quad (14)$$

The goal is to derive the pdf of s, $p(s)$. Some pdfs for a_s are presented in [3]. No expression is available for the pdf of a_c, but the desired goal can be achieved through the pdf of $(h\delta_\ell)$, Eq. 12, and a more general expression for a_c in terms of s in Eq. 13. The latter now is to be achieved by considering the changes in laminar burning velocity due to both flame strain and curvature at the appropriate Karlovitz stretch factors and Markstein numbers [2].

Because the Markstein lengths, L_s and L_c and Markstein numbers, Ma_s and Ma_c are different for strain and curvature [2, 16] the changes in the stretched laminar burning velocity due to the two components are given by

$$u_\ell - u_n = L_s a_s/\tau_\eta + L_c a_c/\tau_\eta. \quad (15)$$

The division of a_s and a_c by τ_η yields the localised dimensional contributions of strain rate and curvature to the flame stretch rate. It follows that

$$\frac{u_\ell - u_n}{u_\ell} = \frac{L_s}{\delta_l}\frac{\delta_\ell}{u_\ell}\frac{a_s}{\tau_\eta} + \frac{L_c}{\delta_\ell}\frac{\delta_\ell}{u_\ell}\frac{a_c}{\tau_\eta}. \quad (16)$$

From Eq. 5 and the definitions of Markstein numbers, $L_s/\delta_\ell = Ma_s$ and $L_c/\delta_\ell = Ma_c$

$$\frac{u_n}{u_\ell} = 1 - K\sqrt{15}[Ma_s a_s + Ma_c a_c]. \quad (17)$$

Evaluation of u_n/u_ℓ in terms of K, Markstein numbers and s could provide, in Eq. 13, a tractable expression for a_c

To this end, Eqs. 14 and 17 give

$$\frac{u_n}{u_\ell} = 1 - sMa_s K\sqrt{15}\left[1 - \frac{a_c}{s}\left(1 - \frac{Ma_c}{Ma_s}\right)\right]. \quad (18)$$

3.2. Values of Markstein numbers

Two problems are associated with Eqs. 1 and 18. They arise because the flame has a finite thickness and because both the flame stretch rate and associated burning velocity depend upon the surface at which they are evaluated. Deshaies and Cambray [17] in their experimental study of stationary, axisymmetric, stretched, laminar burner flames pointed out that this reference surface must be selected with a location accuracy greater than the flame thickness.

Originally, the surface selected by Clavin and Joulin [18] for Eq. 1 was that where the extrapolated spatial temperature profile of the preheat zone reached the burned gas temperature. This approximated the location of the reaction zone. The velocity profile ahead of the flame, when extrapolated through the preheat zone up to this surface gave, at the surface, the burning velocity. This surface was the reference surface subsequently used by Deshaies and Cambray. They found that the value of the strain rate contribution to the flame stretch rate remained unchanged throughout the extrapolated velocity profile. With the flame curvature contribution to the flame stretch rate measured by laser tomography, the surfaces at which the burning velocity and flame stretch rate were measured were almost coincident. Plots of burning velocity against flame stretch rate at this surface were linear and the gradient yielded the Markstein length.

In contrast, Wu and Law [19] in experimental studies of stretched planar burner flames selected a reference surface at the start of the preheat zone. The burning velocity was taken to be the minimum gas velocity at the start of the zone with the strain rate measured just ahead of the selected surface. Plots of burning velocity against flame stretch rate at this reference surface were again linear. However, it is shown in [17] that for a lean propane mixture, with the reference surface at the start of the reaction zone, the Markstein length was positive, but with the reference surface at the start of the preheat zone, it was negative, a natural consequence of the different locations of the surface.

A similar dichotomy arises with explosion flames. The computational study of methane-air spherical explosion flames in [2] shows that with the reference surface located at the beginning of the preheat zone the associated Markstein length is negative. The corresponding burning velocity expresses the rate of accumulation of both unburned and burned gas behind the surface. Alternatively, the burning velocity may be expressed solely in terms of the rate of accumulation of burned gas and the gas in the preheat zone neglected, in which case the associated Markstein length is positive. This is tantamount to locating the reference surface at the start of the reaction zone not only for the burning velocity, but also for the flame stretch rate, as this is independent of the chosen isotherm.

More recently Davis et al. [20] have expressed the view that the Markstein number when defined by the cold boundary is not a physicochemical property of the mixture and that the correct reference surface should lie within the thin fuel consumption zone. Accordingly, u_n/u_ℓ in Eq. 18 first will be evaluated with the reference surface just ahead of the reaction zone and later just ahead of the preheat zone. Further suffices "r" and "p" will indicate Markstein numbers with the reference surface just ahead of these zones, respectively.

Some simplification of Eq. 18 is possible. Referred to the start of the reaction zone as the reference surface, computed values of the Markstein number ratio, now Ma_{cr}/Ma_{sr}, for CH_4-air [2] and C_3H_8-air [21] laminar flames suggest an approximate mean value of this ratio of 0.7 between equivalence ratios of 0.7 and 1.2 for C_3H_8 and of 0.7 and 1.4 for CH_4. At the negative values of Ma_{sr} at the higher equivalence ratios for C_3H_8 this ratio is about 2.9. With regard to a_c/s, because the mean value of $(h\delta_\ell)$ is close to zero, the curvature contribution to the flame stretch rate must be relatively small. Estimates of the approximate magnitude of a_c/s, which is small but variable across the spectrum of stretch values, were obtained from theoretical considerations of the effects of positive curvature in spherical explosions [2] and of negative curvature in cylindrical implosions. For values of $(h\delta_\ell)$ of 0.025 and a density ratio of unburned to burned gas of 6, a_c/s has a value of about 0.37, which decreases towards about 0.17 as the curvature tends to zero. With a value of 0.25 for a_c/s and of 0.7 for Ma_{cr}/Ma_{sr}, Eq. 18 gives

$$\frac{u_n}{u_\ell} = 1 - sMa_{sr}CK\sqrt{15}, \quad (19)$$

in which the numerical constant C is 0.925. For negative values of Ma_{sr} and a value of 2.9 for Ma_{cr}/Ma_{sr}, the value of C is 1.48.

With the preheat zone selected as the reference surface, computed values of the Markstein number ratio, now Ma_{cp}/Ma_{sp}, also can be expressed in terms of the more widely used Markstein numbers, Ma_{sr} and Ma_{cr}. From Eqs. 60 and 61 in [2], it can be shown that

$$Ma_{sp} = Ma_{cp} - \tau(Ma_{sr} - Ma_{cr}), \tag{20}$$

where $\tau = \rho_u/\rho_b - 1$, in which the ratio is that of the unburned to burned gas density. With Eq. 20, Eq. 18 becomes

$$\frac{u_n}{u_\ell} = 1 - \tau s Ma_{sr} K\sqrt{15}\left[-1 + \frac{Ma_{cp} + \tau Ma_{cr}}{\tau Ma_{sr}} + \frac{a_c}{s}\left(1 - \frac{Ma_{cr}}{Ma_{sr}}\right)\right]. \tag{21}$$

Again some simplification is sought. Computed values of $(Ma_{cp} + \tau Ma_{cr})/(\tau Ma_{sr})$ for CH_4-air and C_3H_8-air laminar flames suggest an approximate mean value of this ratio of 0.8 between equivalence ratios of 0.7 and 1.2 for C_3H_8 and of 0.7 and 1.4 for CH_4. For negative values of Ma_{sr} at the higher equivalence ratios for C_3H_8, this ratio is about 2.7. Again with values of 0.25 for a_c/s and of 0.7 for Ma_{cr}/Ma_{sr}, Eq. 21 gives

$$\frac{u_n}{u_\ell} = 1 - \tau s Ma_{sr} CK\sqrt{15}, \tag{22}$$

in which the numerical constant C is -0.125. For negative values of Ma_{sr} and a value of 2.9 for Ma_{cr}/Ma_{sr} and 2.7 for $(Ma_{cp} + \tau Ma_{cr})/(\tau Ma_{sr})$, the value of C is 1.225.

In the case of Eq. 19, u_n/u_ℓ becomes zero at a critical flame stretch rate, s_c:

$$s_c = (Ma_{sr} CK\sqrt{15})^{-1} \tag{23a}$$

and, in the case of Eq. 22 when

$$s_c = (\tau Ma_{sr} CK\sqrt{15})^{-1}. \tag{23b}$$

The right sides of Eqs. 19 and 22 are similar to the factor, f_d, employed by Kostiuk and Bray [7] for u_n/u_ℓ. It expresses a linearity of burning rate that extends over both positive and negative flame stretch rates. This linearity has been confirmed in direct numerical simulations by Chen and Im [4]. Equations 13, 14, and 19 give

$$a_s = s + 2sMa_{sr}C\cdot(h\delta_\ell) - \frac{2(h\delta_\ell)}{K\sqrt{15}}, \tag{24a}$$

for the reaction zone surface. Equations 13, 14, and 22 give

$$a_s = s + 2\tau sMa_{sr}C(h\delta_\ell) - \frac{2(h\delta_\ell)}{K\sqrt{15}}, \tag{24b}$$

for the preheat zone surface. Both equations must employ the appropriate numerical values of C and the last two terms in them are equal to a_c. The equations provide the necessary link between the variables a_s and $(h\delta_\ell)$, the pdfs of which are known, and s, the pdf of which is required.

4. Generation of flame stretch rate PDFS

4.1. Strain rate pdf

For three-dimensional, stationary, isotropic turbulence, the direct numerical simulations of Yeung et al. [3] present pdfs of strain rate for both randomly orientated and material surfaces. Near-Gaussian fits to the two pdfs are employed in the present study. When u_ℓ is smaller than ν_η, the Kolmogorov velocity, there is time for a propagating flamelet surface to align with a strained material surface. On the other hand, when u_ℓ is greater than ν_η there is less time for such alignment and the flamelet surface tends to a random orientation with a mean strain rate of zero [22]. Following Yeung et al. strain and stretch rates have been normalized by multiplying them by the Kolmogorov time, τ_η, to give dimensionless strain rates, a_s. It follows from Eq. 5 that the rms strain rate on a randomly orientated surfaces, u'/λ, when normalized, becomes $(15)^{-1/2} = 0.258$.

The resulting asymmetric, near-Gaussian, general form of $p_2(a_s)$, formulated in [9] and [23] for a surface skewed towards positive strain, is given by

$$p_2(a_s) = \frac{1}{(2\pi)^{1/2}\sigma_s}\exp\left[-\left(\frac{a_s - \bar{a}_s}{2^{1/2}\sigma_s}\right)^2\right]. \tag{25}$$

From [3] for a *material surface* the mean value of dimensionless strain rate, $\bar{a}_s$, is 0.279 and the rms value, σ_s, is 0.341. For a *randomly orientated surface* these values are 0 and 0.258, respectively. In [23] it is shown that the two associated distributions, $p_2(a_s)$, are close to those computed by Yeung et al. Whether, in a flame with the dimensionless rms strain rate for a randomly orientated surface of 0.258, $p_2(a_s)$ should assume the form for a material or randomly orientated surface, depends upon the relative magnitudes of u_ℓ and ν_η.

It can readily be shown that when $u_\ell = \nu_\eta$, $K = 0.258$. In [23] transitional values of $\bar{a}_s$ and σ_s were proposed, between those for a randomly orientated surface at $K = 0$, and those for an assumed material surface at $K = 0.258$ and higher values. These were empirically taken to be

$$\bar{a}_s = [0.279 \exp - (0.0132/K)] \tag{26}$$

$$\text{and } \sigma_s = [0.258 + 0.0826 \exp - (0.0132/K)]. \tag{27}$$

4.2. Stretch rate pdf

In terms of the parameters in both of Eqs. 24 the pdfs of a_s and $(h\delta_\ell)$ are known and the task is to combine them to obtain the pdf of s. It is assumed that $p_2\,(a_s)$ and $p_1\,(h\delta_\ell)$ are statistically independent of each other and that their product is the joint pdf of strain and curvature. There is evidence of this independence from both direct numerical simulations [7] and experiments [12]. Following Kostiuk and Bray [7], a dummy variable, x, is introduced, later to be substituted by $x = (h\delta_\ell)$. It follows from the statistical independence that the joint pdf, $p(s, x)$, is given by [24]

$$p(s, x) = p_2\,(a_s)\; p_1\,(h\delta_\ell) \left| \frac{\partial(a_s,\, (h\delta_\ell))}{\partial(s,\, x)} \right|. \tag{28}$$

The last term on the right is the absolute value of the Jacobian of transformation in which a_s, $(h\delta_\ell)$, and s are continuous random variables. For the reference surface at the reaction zone, with Eq. 24a and $x = (h\delta_\ell)$, it is expressed by

$$\begin{vmatrix} \dfrac{\partial a_s}{\partial s} & \dfrac{\partial a_s}{\partial x} \\ \dfrac{\partial (h\delta_\ell)}{\partial s} & \dfrac{\partial (h\delta_\ell)}{\partial x} \end{vmatrix} = |1 + 2Ma_{sr}C(h\delta_\ell)|. \tag{29}$$

Equations 28 and 29, together with a_s from Eq. 24a and integration with respect to $h\delta_\ell$, give $p_3(s)$, the pdf of normalized flame stretch rate as

$$p_3\,(s) = \int_{-\infty}^{+\infty} |1 + 2Ma_{sr}C(h\delta_\ell)| \cdot p_2\,(a_s)\; p_1\,(h\delta_\ell) \cdot d(h\delta_\ell). \tag{30a}$$

Equation 30a was evaluated numerically for ranges of values of Ma_{sr}, K, and R_l (see Eq. 12), the curvature pdf of Eq. 12 and the strain rate pdf of Eqs. 25–27. Integration with respect to $(h\delta_\ell)$ and the generation of $p_3(s)$ was between the two infinity limits. Adaptive meshing was employed, sufficiently fine to ensure $p_3(s)$ always had an integrated area of unity. Appropriate values of C were selected, as previously discussed.

With the reference surface located at the start of the preheat zone, with Eq. 28 but now invoking Eq. 24b, for that surface for a_s

$$p_3\,(s) = \int_{-\infty}^{+\infty} |1 + 2\tau Ma_{sr}C(h\delta_\ell)| \cdot p_2\,(a_s) p_1(h\delta_\ell) \cdot d(h\delta_\ell), \tag{30b}$$

with the appropriate values of C. Results for both reference surfaces are presented in the next section.

5. Presentation and discussion of computed flame stretch rate PDFS

5.1. Relationship to previous work

The present study covers quite high values of K and R_l, such as might be encountered in practical combustors. However, it must be remembered that the results rest on the DNS-generated strain rate distribution, $p_2\,(a_s)$, of Yeung et al. [3]. In these simulations the Taylor scale Reynolds number, R_λ, ranged from 38–93 (R_l from 90–540). When normalized by Kolmogorov scales, none of the surface properties displayed any significant dependence on Reynolds number. Physically, this is not surprising and it is probably valid to use the pdfs of strain rate at higher Reynolds numbers. Similarly, $p_1\,(h\delta_\ell)$, in Eq. 12, in some instances, will be employed outside the range over which its validity has been established.

The DNS solutions presented by Bray and Cant in [8] are, inevitably, for rather low Reynolds numbers, $R_\lambda = 6.4$ ($R_l = 2.56$) and $Ka = 0.41$ ($K = 0.106$). Their simulated strain rate pdfs are comparable to those in [3]. However, the range of the computed pdfs of curvature, subsequently employed by Kostiuk and Bray [7], is restricted by the DNS, in contrast to the wider range of experimentally based pdfs of curvature of the present study. There is no reference to Reynolds numbers in [7], but the maximum value of Ka is 1.0 ($K = 0.258$) and the values of Markstein numbers, M_d, employed are equivalent to values of Ma_{sr} between — 2.02 and 3.24. Derived pdfs of flame stretch rate are presented in [7] for different values of Ka and M_d. Stretch rates are normalized, not by τ_η, but by the chemical time, δ_ℓ/u_ℓ. Consequently, the profiles of their pdfs are always dependent upon Ka.

5.2. Present stretch rate pdfs

With regard to the present work, profiles of the pdf of flame stretch rate, $p_3(s)$, given by Eq. 30a, for the reference surface at the reaction zone, and evaluated as described at the end of the previous section, are shown in Fig. 5 for a value of Ma_{sr} of unity. Solutions as $p_2\,(a_s)$ tends to the expression for a

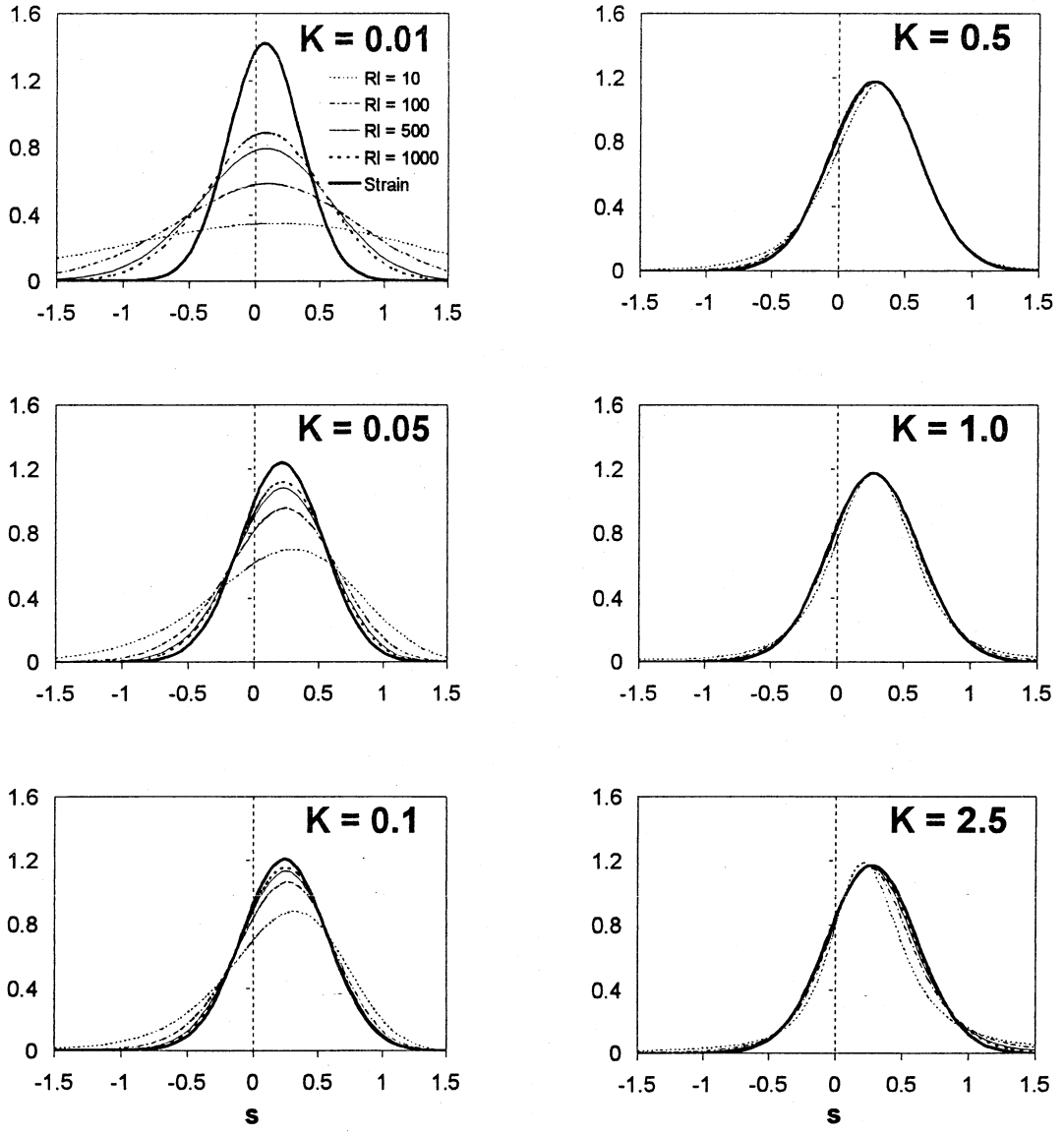

Fig. 5. Dependence of $p_3(s)$ upon K, given by Eq. 30a at $Ma_{sr} = 1$, for $R_l = 10$, 100, 500, and 1000. Strain rate pdf, $p_2(a_s)$, given by Eqs. 25–27 (bold curve).

randomly orientated surface at $K = 0$ are shown in the left column for $K \leq 0.10$. Those as the pdf tends to the expression for a material surface are shown in the right column for $0.5 \leq K \leq 2.5$. The strain rate pdfs, p_2 (a_s), given by Eqs. 25– 27 are shown bold in all the figures. The pdfs of flame stretch rate, p_3 (s), for different values of K are given for four different values of R_l. It can be seen that when $K \leq 0.05$ there is a greater spread of stretch rates than at the higher values of K. It was found that for $K \geq 0.25$ and $R_l \geq 100$, p_3 (s) is close to p_2 (a_s) and they tended to become coincident at the higher values of R_l. On the other hand, at low values of $K \leq 0.25$ and at all values of R_l, p_3 (s) is very dependent upon both of these parameters. As the value of K decreases to small values, the influence of flame curvature increases. This broadens the spread of stretch rates, particularly at low R_l, significantly beyond those due to strain rate alone.

In comparison, it can be seen from Fig. 6 for a negative value of Ma_{sr}, $= -1$, that the effect of curvature on p_3 (s) is rather more marked. This is particularly so at the lowest values of K and the lowest value of R_l of 10. For the lower range of K

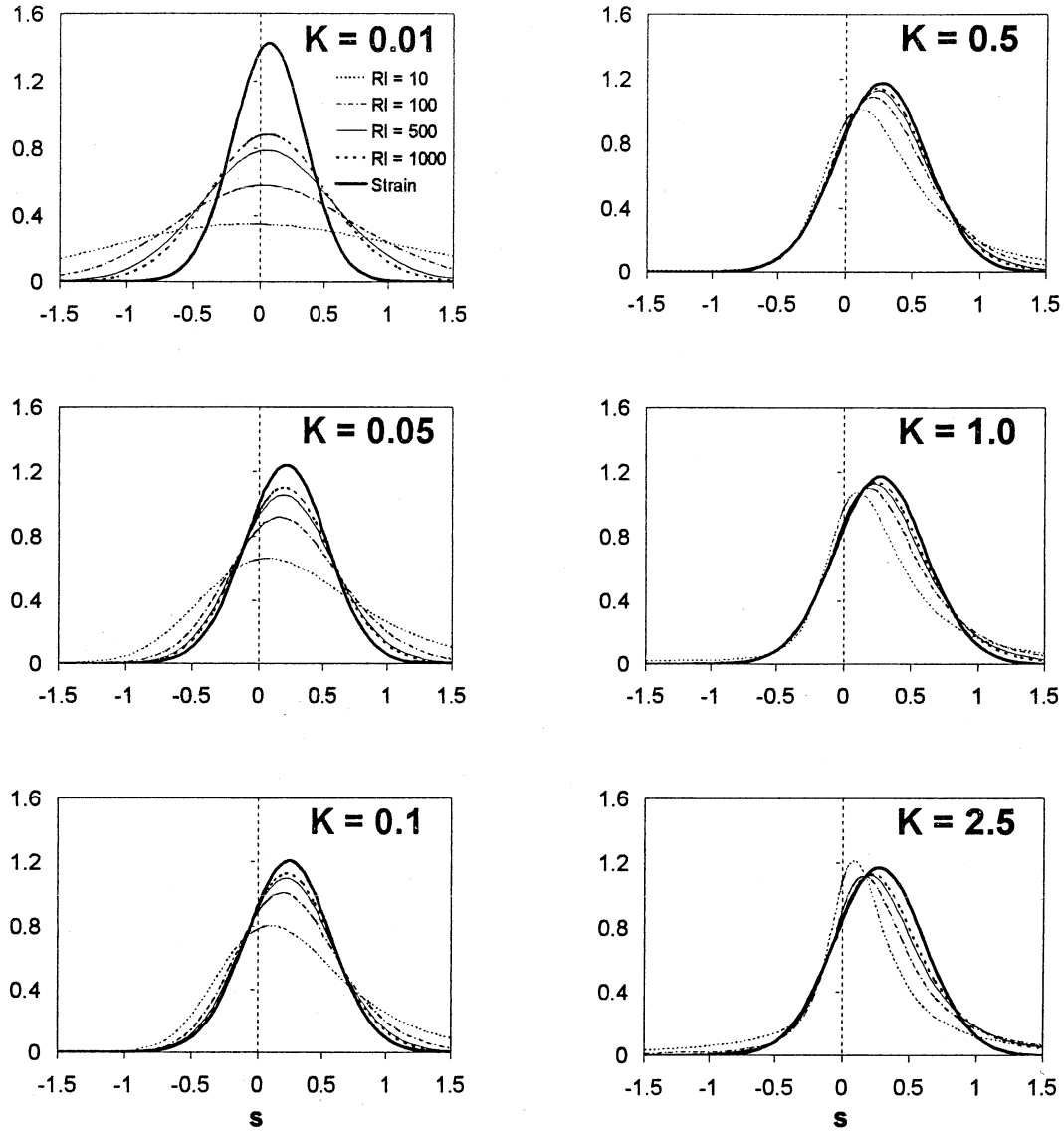

Fig. 6. Dependence of $p_3(s)$ upon K, given by Eq. (30a) at $Ma_{sr} = -1$, for $R_l = 10$, 100, 500, and 1000. Strain rate pdf, $p_2(a_s)$, given by Eqs. 25–27 (bold curve).

values, as the random orientation is approached, there is some skewing of the distribution towards negative stretch rates at low R_l.

Profiles of p_3 (s) at the rather more commonly encountered value of $Ma_{sr} = 4$ are given in Fig. 7, again for the stretch rate reference surface at the reaction zone. Particularly at the lower values of K and R_l, at $K = 0.01$ and 0.05, although the peak values of p_2 (a_s) are greater than those of p_3 (s), there is an increase of p_3 (s) above p_2 (a_s) in a longer tail of negative stretch rate, arising from the curvature contribution to the flame stretch rate. This also was observed in the numerical simulations of Chen and Im [4]. In Fig. 7 the peak of p_3 (s) is skewed to positive values. For values of K greater than 0.5, the peak values of p_3 (s) are greater than those of p_2 (a_s) and occur at lower values of s. These changes are associated with the change in sign of u_n/u_ℓ to negative values at values of s, above the critical flame stretch rate, s_c, given by Eq. 23a. This equation also shows this limit to be inversely proportional to K. For example, with $Ma_{sr} = 4$ and $C = 0.925$, u_n/u_ℓ becomes negative with $K = 0.1$ when $s \geq 0.7$ and with $K = 1.0$ when $s \geq 0.07$.

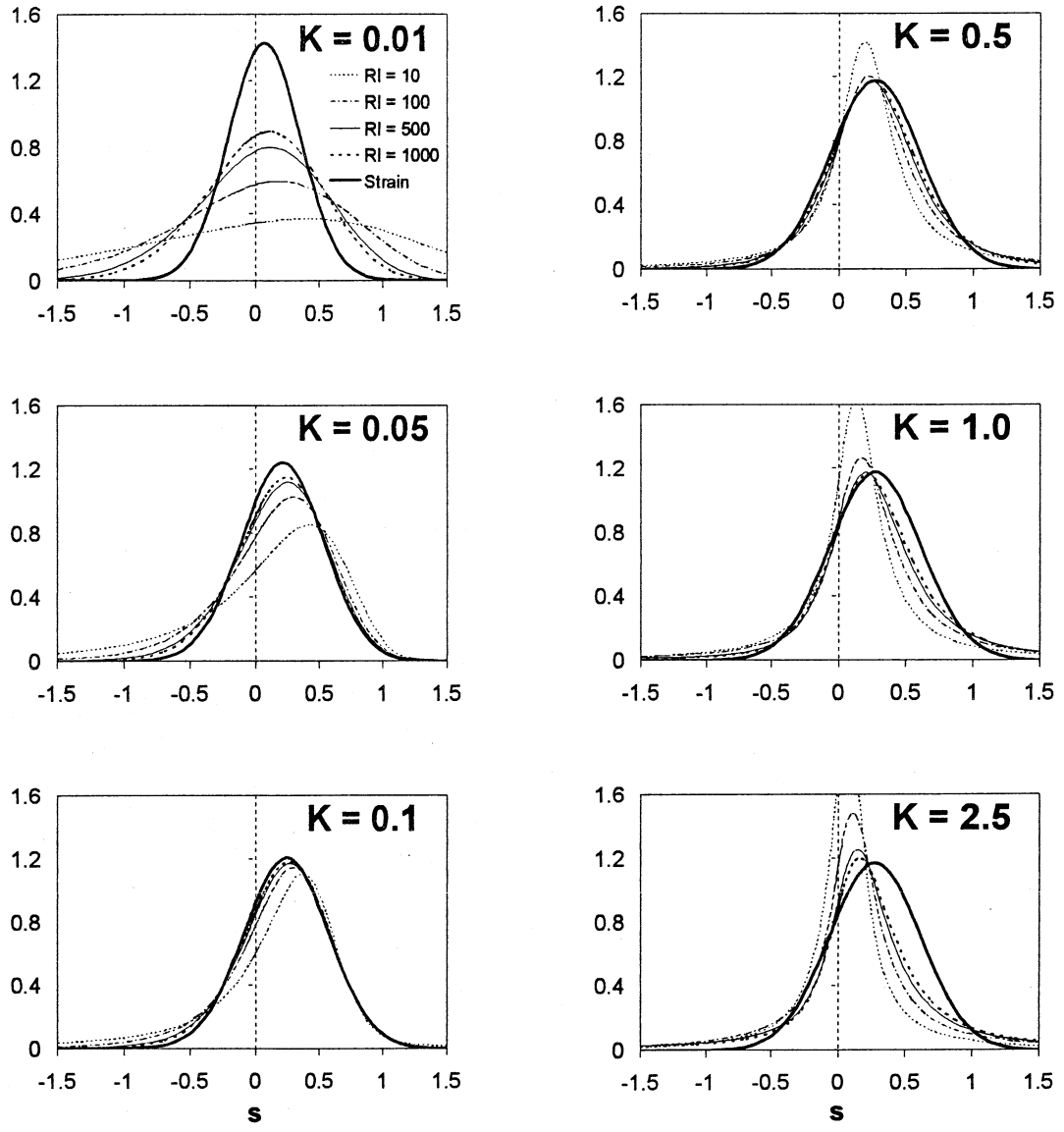

Fig. 7. Dependence of $p_3(s)$ upon K, given by Eq. 30a at $Ma_{sr} = 4$, for $R_l = 10$, 100, 500, and 1000. Strain rate pdf, $p_2(a_s)$, given by Eqs. 25–27 (bold curve).

Instances of what are variously called "negative flame speeds," "negative flames," "negative burning velocities," and "negative displacement speeds" appear in the literature. In the careful experiments of Sohrab et al. [25] on different types of laminar counter-flow flames, a weak ancillary flame is generated above the stagnation plane. There is a diffusive flux of reactants to this flame from the cold mixture flow beneath the plane. Above the ancillary flame is the principal stoichiometric flame, from which hot products flow downwards and from which also energy is conducted, to the ancillary flame. As a consequence, the stabilised ancillary becomes a negative flame propagating *into,* not *away from,* the hot products. The DNS of Chen and Im [4] also demonstrate how a diffusive flux tangential to a flame front can exceed an adverse convective flux, to create a "negative flame" that propagates *into* the hot products.

It would appear that such negative flames only exist as ancillaries to other flames, are super-adiabatic, associated with strong diffusive fluxes, and contribute little to the burning rate. As a consequence, their existence in the present context, does not support the extension of Eq. 19 into a regime of

negative values of u_n/u_ℓ. Instead, it is assumed that although this ratio describes the linear variation of positive values of u_n/u_ℓ with s, a limiting condition is approached in which the flame approaches extinction and u_n/u_ℓ tends towards a value of zero. It follows from Eq. 13 that a_c also must tend to zero. However, it also follows that it is no longer valid for Eqs. 19 and 24a to be used as continuous functions. Consequently Eqs. 28–30b can neither be applied, nor rigorously amended.

Nevertheless, the condition $a_c \to 0$ as s exceeds s_c also implies $s \to a_s$. A not surprising consequence of this, confirmed by numerical studies, is that in this regime, as s increases, values of $p_3(s)$ tend towards those of $p_2(a_s)$. The two pdfs become closer than is suggested by the solutions of Fig. 7 that are based on u_n/u_ℓ becoming negative in the linear relationship of Eq. 19. The apparent greater deviation of $p_3(s)$ from $p_2(a_s)$ as K is increased can be explained by the associated decrease in s_c. Above the positive value of s_c as $s \to a_s$, $p_3(s)$ will tend towards $p_2(a_s)$. For the integrated area under $p_3(s)$ to remain unity, the increases in the values of the pdf at values of s above s_c must be compensated by decreases in the values below s_c. In this way $p_3(s)$ comes close to $p_2(a_s)$ over the range $K \geq 0.1$ and $R_l \geq 100$. Differences between the two pdfs are more apparent than real and are a consequence of the inability of Eqs. 28–30b to deal with discontinuous functions.

For the highly negative value of Ma_{sr}, $= -4$, the departures of $p_3(s)$ from $p_2(a_s)$ are more marked, even with $R_l \geq 100$, as can be seen from Fig. 8. The skewing of the profiles at the lower values of K is opposite to that with a positive value of Ma_{sr}. Again, the greatest differences between $p_3(s)$ and $p_2(a_s)$ occur at $K = 0.01$ and 0.05, but in this case there is a long tail of *positive* stretch rate. As with $Ma_{sr} = 4$ the peak values of $p_3(s)$ become greater than those of $p_2(a_s)$ as K increases, but these now occur at somewhat lower values of s. As before, it would appear that this is associated with u_n/u_ℓ in Eq. 19 becoming negative, at values of s beyond s_c.

With $Ma_{sr} = -4$ and $C = 1.48$, u_n/u_ℓ would become negative with $K = 0.1$ when s is less than the critical value, $s_c = -0.44$. With $K = 0.1$, $s_c = -0.044$. Imposing an extinction flame with $u_n/u_\ell \to 0$ at less than these critical values of s in preference to allowing negative flames, as before, would suggest $a_s \to s$ and $p_3(s) \to p_2(a_s)$. For the integrated area under the pdf profile to be unity, the reductions in the computed $p_3(s)$ in Fig. 8 below the critical value of s would lead to a corresponding increase in $p_3(s)$ above this value. As before, these considerations lead to the two pdfs becoming closer when $R_l \geq 100$, while the biggest differences between them remain at $K \leq 0.05$.

The effects of different values of Ma_{sr}, ranging from -4 to 12, are shown rather more clearly in Fig. 9. Here the left column is for an almost randomly orientated surface, $K = 0.01$, and the right column is for a predominantly material surface, $K = 1.0$. The computations cover four values of R_l. Not surprisingly, the influence of both curvature and Ma_{sr} is greatest when K and R_l are small. For values of R_l of 100 and above, the stretch pdfs are less sensitive to Ma_{sr}. For the higher value of K the $p_3(s)$ profile is closest to that of $p_2(a_s)$ for Ma_{sr} values between -1 and 4. If negative flames were to be proscribed, higher positive values of Ma_{sr} would result in lower values of s_c for extinction flames. As before, this would bring $p_3(s)$ closer to $p_2(a_s)$. These considerations tend to reduce the apparent effects of Ma_{sr} in Fig. 9.

Computations of $p_3(s)$ also were made with the reference surface at the start of the preheat zone and employing Eq. 30b, instead of Eq. 30a. In general, because C in Eq. 22 is negative, in contrast to C in Eq. 19, the value of s at which $p_3(s)$ peaks with this reference surface is less positive than that with the reaction zone surface. This can be seen by comparing Fig. 10 for $Ma_{sr} = 1$ and $\tau = 6$ with Fig. 5. This change in the sign of C is similar to one in the sign of Ma_{sr}, particularly at low values of K, as can be seen by comparing Fig. 10 with Fig. 6. Otherwise, with the preheat reference surface and $Ma_{sr} = 1$, as in Fig. 5, when $K \geq 0.25$ and $R_l \geq 100$ $p_3(s)$ is close to $p_2(a_s)$.

The computed profiles of $p_3(s)$ in Fig. 11, for $Ma_{sr} = -1$ and $\tau = 6$ for the preheat zone reference surface differ significantly, not only from those in both Figs. 5 and 6 for the reaction zone surface, but also from $p_2(a_s)$, over wide ranges of K and R_l values. It would seem that the latter surface gives greater generality in $p_3(s)$ than does the former.

Shown in Fig. 12 are the computed profiles of $p_3(s)$ for $Ma_{sr} = 4$ and $\tau = 6$, to be compared with those in Fig. 7. However, as a consequence of the negative values of C (-0.125) in Eq. 24b, the profiles of $p_3(s)$ are rather closer to those with a negative value of $Ma_{sr} = -4$, shown in Fig. 8 for the reaction zone surface. Equation 23b for $K = 1.0$ and $\tau = 6$ gives $s_c = -0.086$. It follows that for more negative values of s, $p_3(s)$ will become closer to $p_2(a_s)$, with a compensatory increase in $p_3(s)$ for positive values of s, again bringing the two pdfs closer.

5.3. Flame instabilities

Earlier studies of spherical laminar flames have shown Darrieus-Landau and thermo-diffusive flame instabilities to occur at a combination of low flame stretch rates and low (particularly negative) Markstein numbers [9,14]. The instabilities wrinkle the

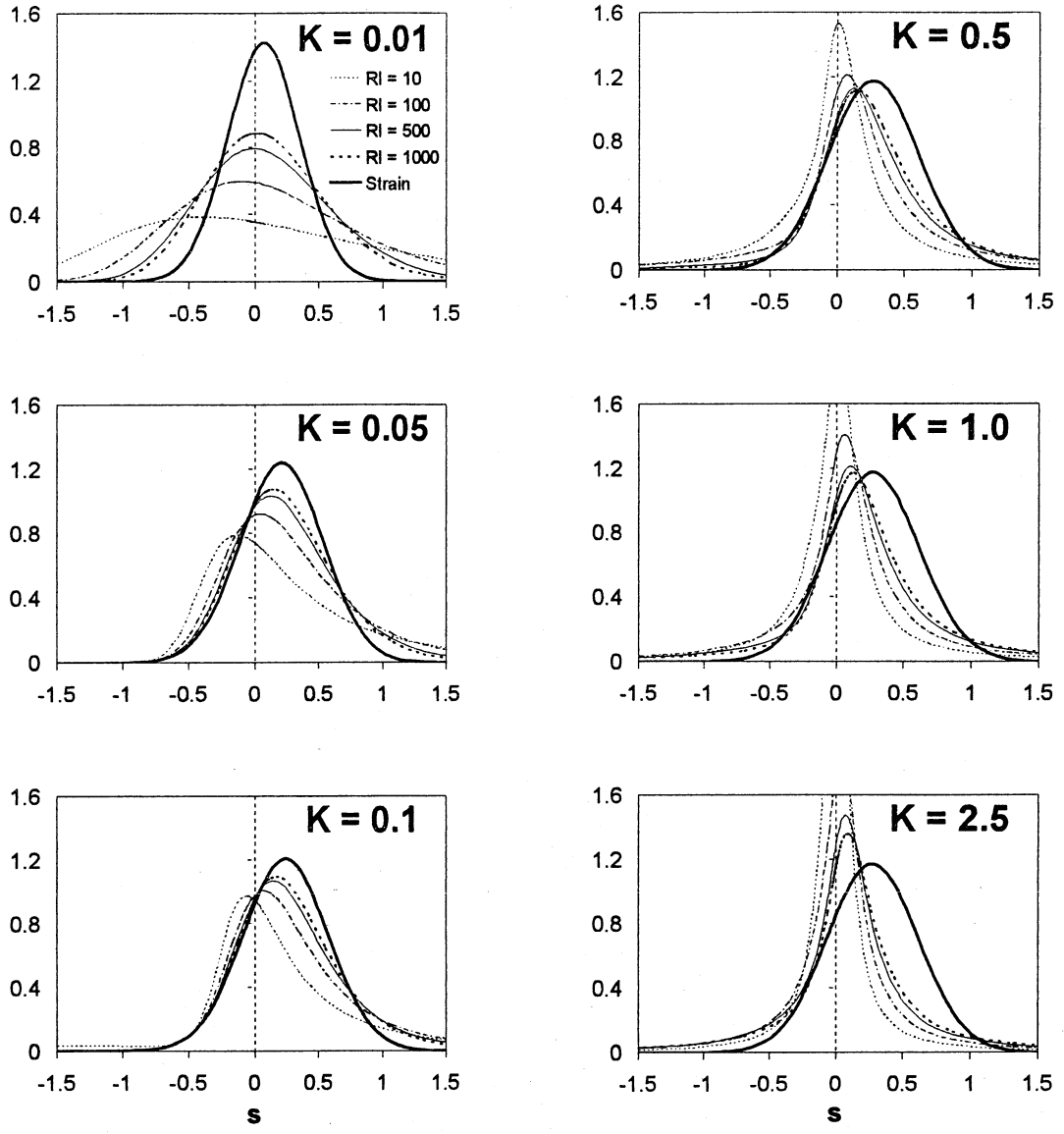

Fig. 8. Dependence of $p_3(s)$ upon K, given by Eq. 30a at $Ma_{sr} = -4$, for $R_l = 10$, 100, 500, and 1000. Strain rate pdf, $p_2(a_s)$, given by Eqs. 25–27 (bold curve).

flame and increase the overall burning velocity. If such instabilities were to occur in laminar flamelets, they might increase the turbulent burning velocity and the mean volumetric heat release rate. Consequently, it is important to identify the regime in which this might occur in turbulent combustion.

An attempt to do this is now made, somewhat simplistically, by considering convex laminar flamelet propagation normal to a spherical surface, radius, r. The dimensional flame stretch rate arising from this is $(\frac{2}{r})\frac{\partial r}{\partial t}$, which can be expressed in the present dimensionless form as

$$s = \frac{2}{r}\frac{\delta_\ell}{u_\ell}\frac{\partial r}{\partial t}\left(\frac{\lambda u_\ell}{u'\sqrt{15}\delta_\ell}\right) = \frac{2}{PeK\sqrt{15}}\left(\frac{1}{u_\ell}\frac{\partial r}{\partial t}\right), \tag{31}$$

in which Pe is the Peclet number $= r/\delta_\ell$, based on localised curvature. At low stretch rates the final

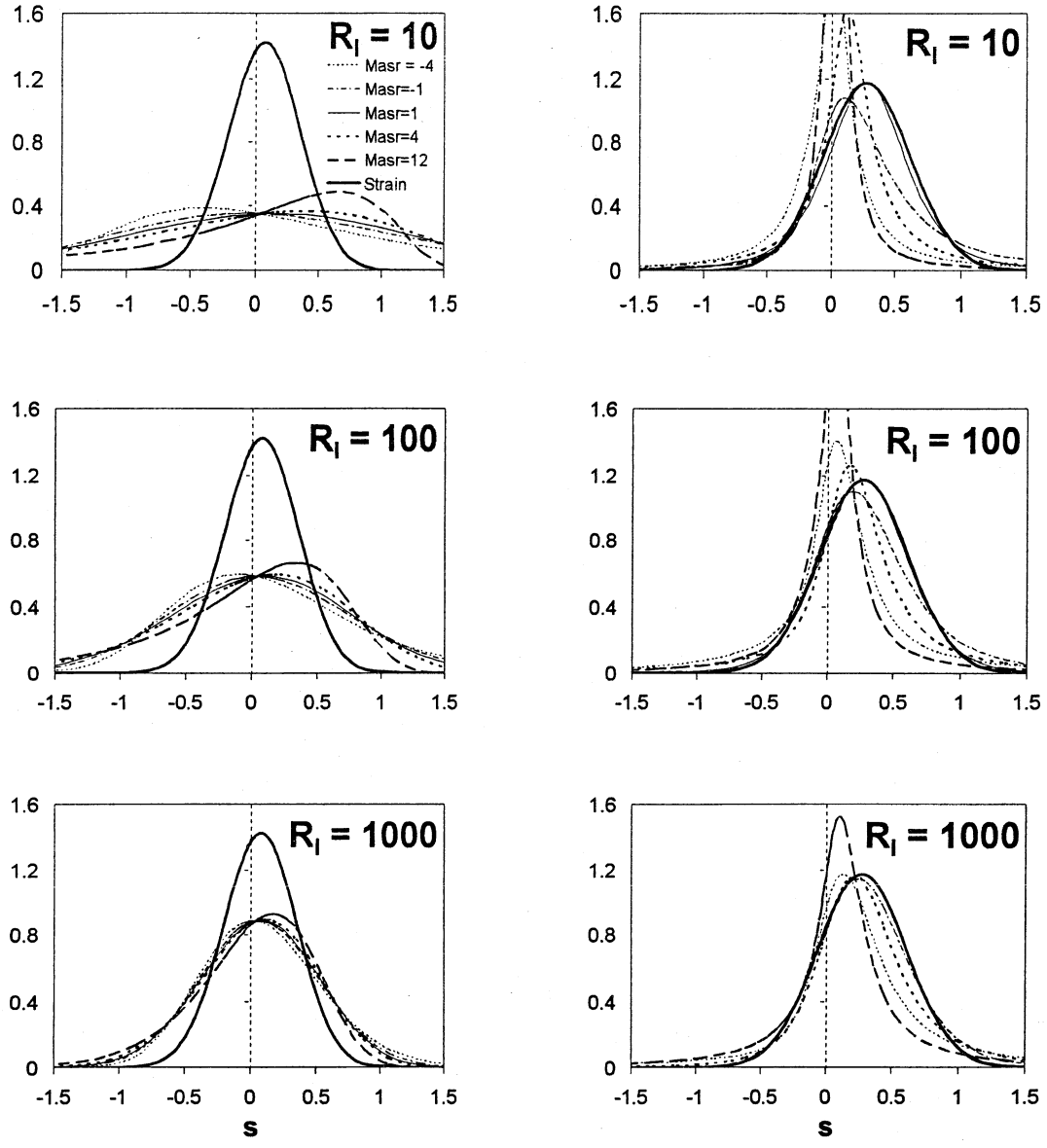

Fig. 9. Dependence of $p_3(s)$ given by Eq. 30a for values of Ma_{sr} from -4 to 12 at $K = 0.01$ (left column) and $K = 1.0$ (right column). $R_l = 10$, 100, and 1000. Strain rate pdf, $p_2(a_s)$, given by Eqs. 25–27 (bold curve).

bracketed term is close to the ratio of unburned to burned gas density, ρ_u/ρ_b.

There is considerable evidence to show that above a critical value of Pe, denoted by Pe_{cl}, a spherical flame under positive stretch becomes unstable, as a consequence of the reduction in flame stretch rate. This implies that there must be a critical value of s, below which, a flamelet would be unstable, namely in Eq. 31, when

$$s \leq \frac{2}{\sqrt{15}Pe_{cl}K}\frac{\rho_u}{\rho_b} = \frac{0.516}{Pe_{cl}K}\left(\frac{\rho_u}{\rho_b}\right). \tag{32}$$

In [14] for the spherical laminar, unstable, iso-octane-air flame, $\phi = 1.5$ at an initial pressure of 0.1 MPa and temperature of 358 K, $Ma_{sr} = -1.6$ and $Pe_{cl} = 295$. With this value of Pe_{cl}, a value of ρ_u/ρ_b for the mixture of 6.71, and a value of K of 0.04, then $s \leq 0.29$. For this value of K in Fig. 6 and $R_l = 100$

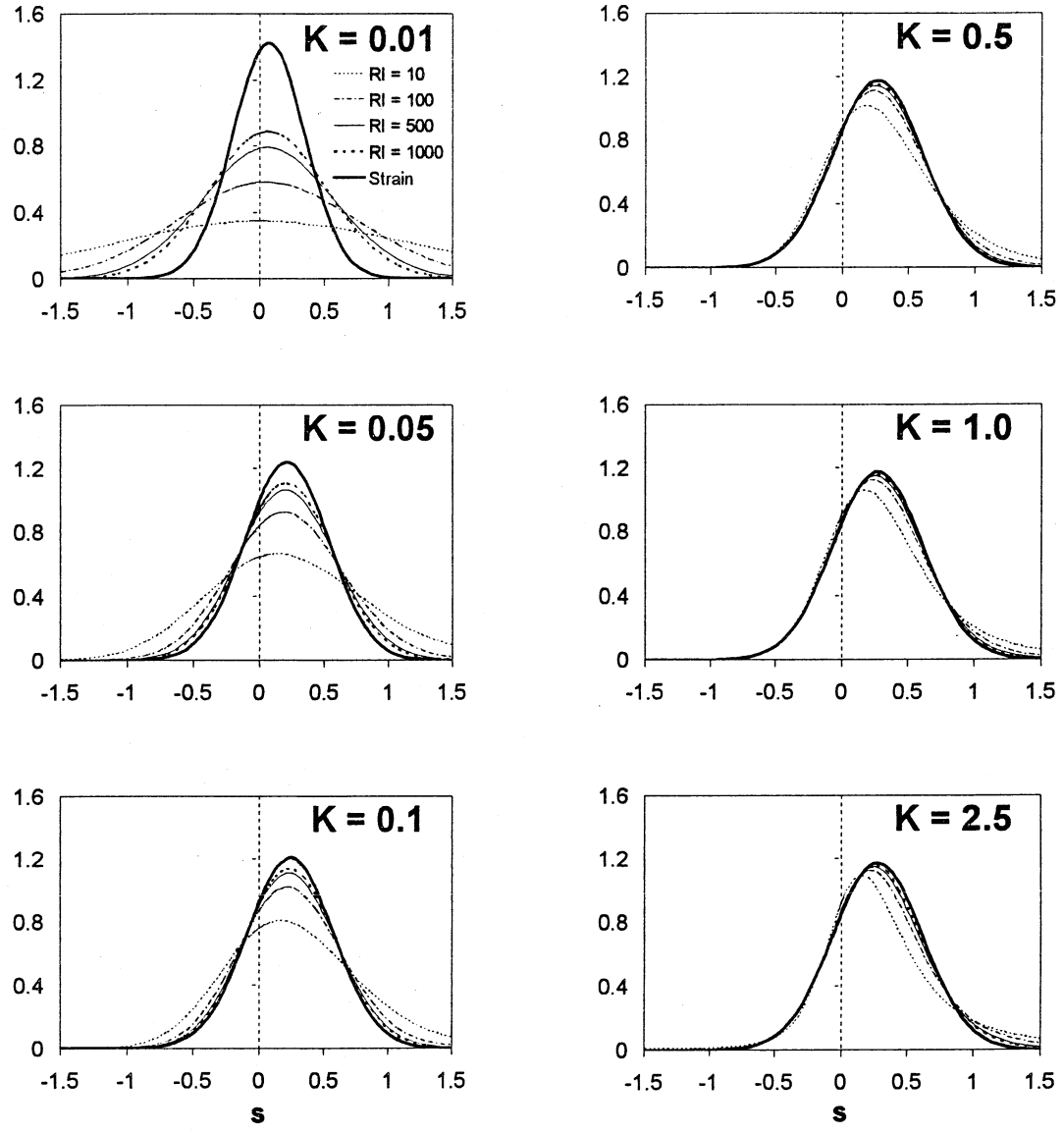

Fig. 10. Dependence of $p_3(s)$ upon K, given by Eq. 30b, for a preheat zone reference surface, at $Ma_{sr} = 1$ with $\tau = 6$, for $R_l = 10$, 100, 500, and 1000. Strain rate pdf, $p_2(a_s)$, given by Eqs. 25–27 (bold curve).

approximately 31% of the spectrum of positive stretch rate might be unstable, at values of s close to zero. About 69% of the spectrum of flame stretch rates, s, is positive.

For more typical turbulent flame conditions, with a positive value of Ma_{sr} and a higher value of K, the flamelets are more stable. For example, with $Ma_{sr} = 4$ (for which $Pe_{cl} = 2885$) and $K = 0.4$, again with $\rho_u/\rho_b = 6.71$, then from Eq. 32 instability only occurs when $s \leq .003$. For this value of K, the data in Fig. 7 suggest a negligible proportion of the spectrum of positive stretch rates might be unstable. The direct numerical simulations of Boughanem and Trouvé [26] also suggest that instabilities become important in turbulent combustion only at low values of both Ma_{sr} and K.

6. Conclusions

A wide range of experimentally determined pdfs of turbulent flame curvature from a variety of sources has been surveyed and a correlating expression derived for these. The expression derived is Eq. 10, but

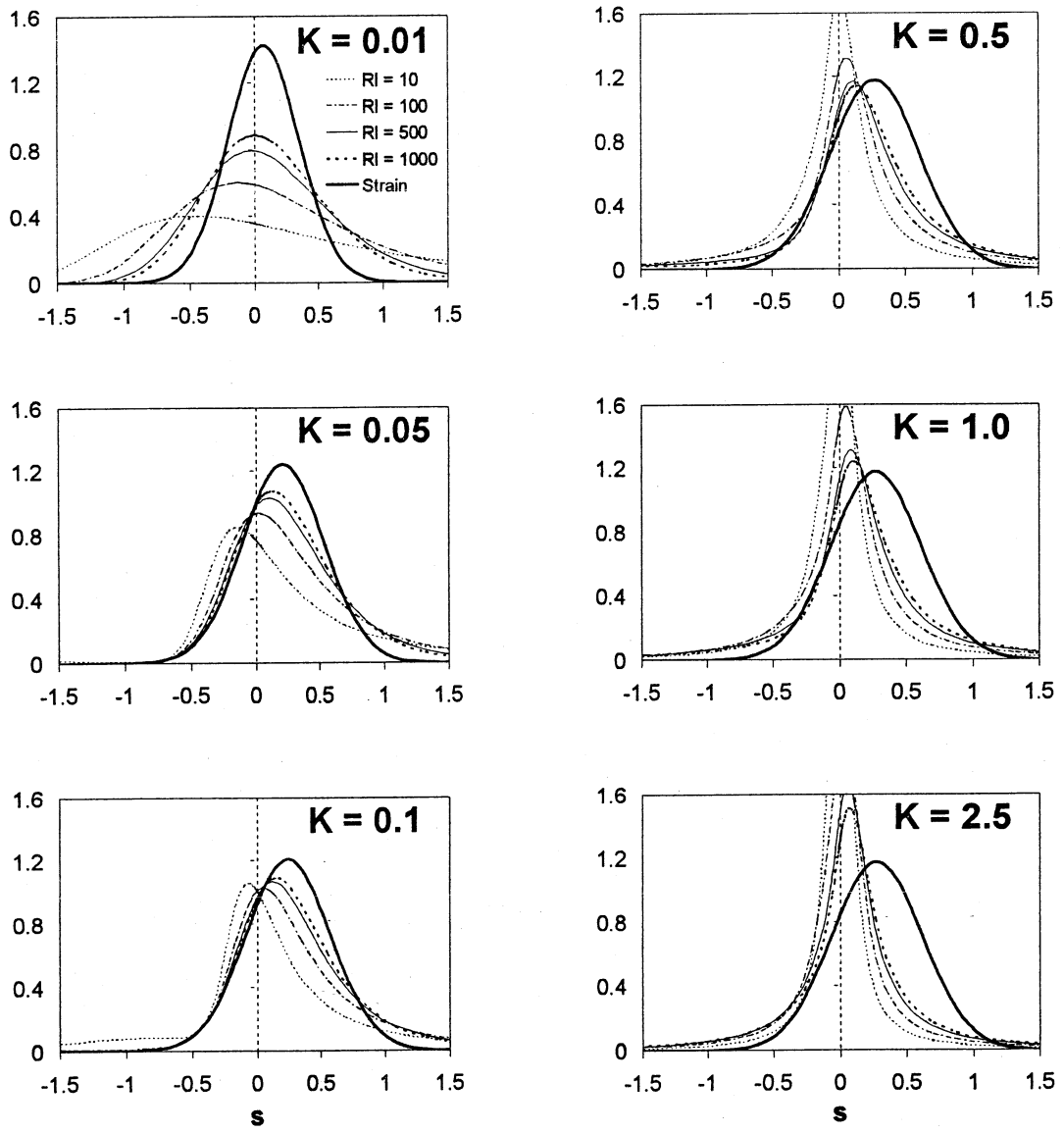

Fig. 11. Dependence of $p_3(s)$ upon K, given by Eq. 30b, for a preheat zone reference surface, at $Ma_{sr} = -1$ with $\tau = 6$, for $R_l = 10$, 100, 500, and 1000. Strain rate pdf, $p_2(a_s)$, given by Eqs. 25–27 (bold curve).

it can also be expressed by Eqs. 11 and 12. The first and last are the more practical forms, but Eq. 11 is of interest physically because it suggests a simple generalisation in terms of curvature normalized by the Taylor scale of turbulence.

Evaluation of u_n/u_l enables the contribution to the dimensionless flame stretch rate because of curvature to be found, in terms of s, Ma_{sr}, K, and the curvature. This relationship, together with the Jacobian of transformation for a_s and $(h\delta_\epsilon)$, the pdfs of which are known, has enabled pdfs of flame stretch rate to be obtained, following the approach of Kostiuk and Bray [7]. Strain rate pdfs, including the transition between material and randomly orientated surfaces were taken from [3] and [23]. Probability density functions for flame stretch rate have been computed over wide ranges of K, R_l, and Ma_{sr}. These cover two different reference surfaces for the burning velocity and stretch rate, namely those just ahead of the preheat and the reaction zones. The latter appears to be more appropriate.

The computations also cover whether, or not, the stretched laminar burning velocity may be negative. It would appear that negative flames are unlikely to

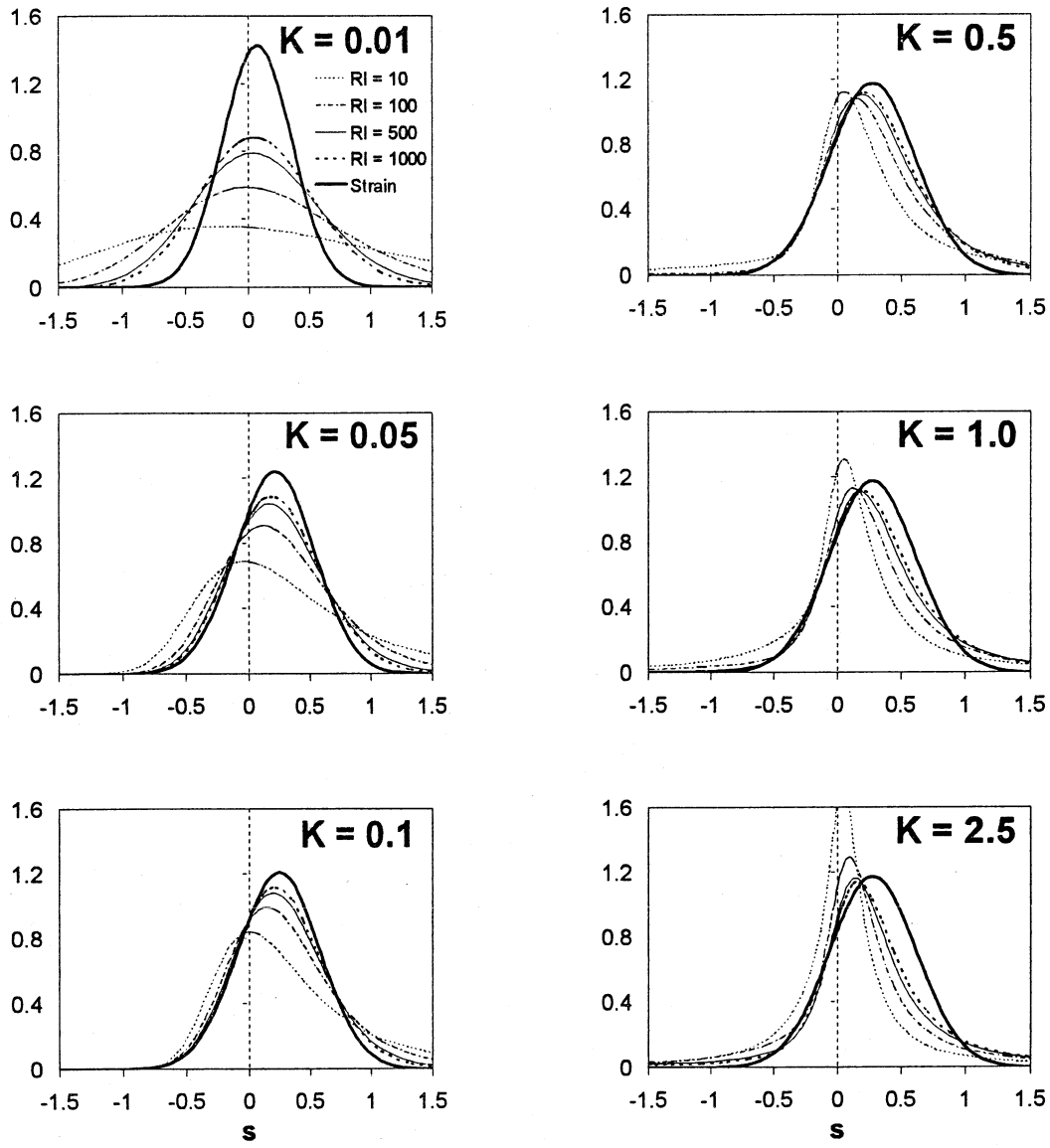

Fig. 12. Dependence of $p_3(s)$ upon K, given by Eq. 30b, for a preheat zone reference surface, at $Ma_{sr} = 4$ with $\tau = 6$, for $R_l = 10$, 100, 500, and 1000. Strain rate pdf, $p_2(a_s)$, given by Eqs. 25–27 (bold curve).

be significant and that a regime associated with a flame approaching extinction with $a_c \rightarrow 0$ and $s \rightarrow a_s$ as $u_n/u_\ell \rightarrow 0$ is more likely. Allowance for this is difficult to quantify accurately because the terms in the Jacobian of transformation are no longer continuous variables. Nevertheless, the numerical solutions suggest that, as K is increased $p_3(s)$ becomes closer to $p_2(a_s)$ over the range $K \geq 0.1$, $R_l \geq 100$, $-1 \leq Ma_{sr} \leq 4$. In this regime the influence of curvature is very small. Greater generality along these lines is achieved with the start of the reaction zone, rather than the start of the preheat zone, as locations for the datum surface.

An important finding is that the influence of curvature is greatest at low values of K and R_l. Not surprisingly, this is where the influence of Ma_{sr} also is greatest. Consideration of the conditions for flame instabilities suggests that these may be pronounced at very low values of K and negative values of Ma_{sr}. They would enhance flamelet wrinkling and hence the volumetric burning rate and turbulent burning velocity.

Acknowledgment

We thank Robert Woolley for his advice on the processing of the experimental pdfs of curvature. The financial support of EPSRC is gratefully acknowledged.

References

[1] S. M. Candel, T. J. Poinsot, Combust. Sci. Tech. 70 (1990) 1.
[2] D. Bradley, P. H. Gaskell, X. J. Gu, Combust. Flame 104 (1996) 176.
[3] P. K. Yeung, S. S. Girimaji, S. B. Pope, Combust. Flame 79 (1990) 340.
[4] J. H. Chen, H. G. Im. Twenty-Seventh Symposium (International) on Combustion, The Combustion Institute, Pittsburgh, 1998, p. 819.
[5] B. Renou, A. Boukhalfa, D. Puechberty, M. Trinité. Twenty-Seventh Symposium (International) on Combustion, The Combustion Institute, Pittsburgh, 1998, p. 841.
[6] C. J. Rutland, A. Trouvé, Combust. Flame 94 (1993) 41.
[7] L. W. Kostiuk, K. N. C. Bray, Combust. Sci. Tech. 95 (1994) 193.
[8] K. N. C. Bray, R. S. Cant, Proc. R. Soc. Lond. A434 (1991) 217.
[9] D. Bradley, Combust. Theory Model. 6 (2002) 361.
[10] M. Z. Haq, C. G. W. Sheppard, R. Woolley, D. A. Greenhalgh, R. D. Lockett, Combust. Flame 131 (2002) 1.
[11] I. G. Shepherd, R. K. Cheng, T. Plessing, C. Kortschik, N. Peters, Proc. Combust. Inst. 29 (2002) 1833–1840.
[12] D. A. Nye, J. G. Lee, T. -W. Lee, D. A. Santavicca, Combust. Flame 105 (1996) 167.
[13] T. -W. Lee, G. L. North, D. A. Santavicca, Combust. Flame 93 (1993) 445.
[14] D. Bradley, C. G. W. Sheppard, R. Woolley, D. A. Greenhalgh, R. D. Lockett, Combust. Flame 122 (2000) 195.
[15] D. W. Marquardt, J. Soc. Industrial Applied Mathematics 11 (1963) 431.
[16] D. Durox, S. Ducruix, S. Candel, Combust. Flame 125 (2001) 982.
[17] B. Deshaies, P. Cambray, Combust. Flame 82 (1990) 361.
[18] Clavin, P. and Joulin, G., J. Phys. Lett. L1–L12 (1983).
[19] C. K. Wu, C. K. Law. Twentieth Symposium (International) on Combustion, The Combustion Institute, Pittsburgh, 1984, p. 1941.
[20] S. G. Davis, J. Quinard, G. Searby, Combust. Flame 130 (2002) 123.
[21] D. Bradley, P. H. Gaskell, X. J. Gu. Twenty-Seventh Symposium (International) on Combustion, The Combustion Institute, Pittsburgh, 1998, p. 849.
[22] S. S. Girimaji, S. B. Pope, J. Fluid Mech. 234 (1991) 247.
[23] D. Bradley, A. K. C. Lau, M. Lawes, Phil. Trans. R. Soc. Lond. A338 (1992) 357.
[24] G. A. Korn, T. M. Korn, Mathematical Handbook for Scientists and Engineers: Definitions, Theorems and Formulas for Reference and Review. Second ed., McGraw Hill, New York, 1968, p. 616.
[25] S. H. Sohrab, Z. Y. Ye, C. K. Law. Twentieth Symposium (International) on Combustion, The Combustion Institute, Pittsburgh, 1984, p. 1957.
[26] H. Boughanem, A. Trouvé. Twenty-Seventh Symposium (International) on Combustion, The Combustion Institute, Pittsburgh, 1998, p. 971.